A&A 399, 1083–1099 (2003)
DOI: 10.1051/0004-6361:20021826

Astronomy & Astrophysics

The association of IRAS sources and ^{12}CO emission in the outer Galaxy⋆

C. R. Kerton[1] and C. M. Brunt[1,2]

[1] National Research Council of Canada, Herzberg Institute of Astrophysics, Dominion Radio Astrophysical Observatory, PO Box 248, Penticton, BC V2A 6J9 Canada
[2] Department of Physics and Astronomy, University of Calgary, 2500 University Dr. NW, Calgary, AB T2N 1N4 Canada

Received 7 October 2002 / Accepted 9 December 2002

Abstract. We have revisited the question of the association of CO emission with IRAS sources in the outer Galaxy using data from the FCRAO Outer Galaxy Survey (OGS). The availability of a large-scale high-resolution CO survey allows us to approach the question of IRAS-CO associations from a new direction – namely we examined *all* of the IRAS sources within the OGS region for associated molecular material. By investigating the association of molecular material with random lines of sight in the OGS region we were able to construct a quantitative means to judge the likelihood that any given IRAS-CO association is valid and to disentangle multiple emission components along the line of sight. The paper presents a list of all of the IRAS-CO associations in the OGS region. We show that, within the OGS region, there is a significant increase (~22%) in the number of probable star forming regions over previous targeted CO surveys towards IRAS sources. As a demonstration of the utility of the IRAS-CO association table we present the results of three brief studies on candidate zone-of-avoidance galaxies with IRAS counterparts, far outer Galaxy CO clouds, and very bright CO clouds with no associated IRAS sources. We find that ~25% of such candidate ZOAGs are Galactic objects. We have discovered two new far outer Galaxy star-forming regions, and have discovered six bright molecular clouds that we believe are ideal targets for the investigation of the earliest stages of sequential star formation around HII regions. Finally, this paper provides readers with the necessary data to compare other catalogued data sets with the OGS data.

Key words. ISM: molecules – infrared: ISM – radio lines: ISM – catalogs – Galaxy: general

1. Introduction

Due to the overwhelming amount of time required to conduct a large-scale survey of the molecular gas distribution in our Galaxy previous high-resolution (~1′) molecular line surveys necessarily made pointed observations toward secondary tracers of molecular gas such as IRAS sources selected on the basis of their colour, flux density quality, and brightness (e.g., Yang et al. 2002; Wouterloot & Brand 1989, WB89 hereafter). While such surveys provide a wealth of information on star formation and the distribution of molecular material in the Galaxy they are clearly biased by the pre-selection of target locations. For example, in the WB89 survey region there are 44 454 IRAS point sources. Application of colour and flux criteria reduce the number of objects examined to 1302 (~3%) and it is not unreasonable to expect that some of the 43152 other objects are also associated with CO. Now that large-scale, unbiased, high-resolution CO surveys are becoming available it is important to revisit the question of the association of IRAS sources and CO.

From 1994–1997 the FCRAO Outer Galaxy Survey (Heyer et al. 1998, OGS hereafter) mapped out the distribution of CO within the Galaxy from $102.^{\circ}49 < l < 141.^{\circ}54$, $-3.^{\circ}03 < b < 5.^{\circ}41$, at 45″ spatial resolution sampled every 50.″22 and 0.98 km s^{-1} velocity resolution (1.39 km s^{-1} for $l < 106^{\circ}$) sampled every 0.81 km s^{-1}. Recently the OGS data were reprocessed (see Sect. 2) and a new high-resolution CO cloud catalogue (Brunt et al. 2003, BKP hereafter) was constructed. The BKP catalogue provides a concise description of the OGS data and thus facilitates the comparison of the OGS data with other catalogued data sets. With the availability of the OGS and the BKP catalogue we were able to approach the question of IRAS-CO associations from a new direction – namely we examined *all* of the IRAS sources within the OGS region for associated molecular material. The resulting IRAS-CO association table is presented in this paper and should be of widespread utility for a number of studies.

In Sect. 2 we first present the data used and the techniques we applied to obtain the IRAS-CO associations. The full table of IRAS-CO associations is provided in the form of an electronic machine-readable table available through the CDS (see Table 1). In an appendix to the paper we explain how one

Send offprint requests to: C. R. Kerton,
e-mail: charles.kerton@nrc.ca

⋆ Tables 1, 2 and A1 are only available in electronic form at the CDS via anonymous ftp to
cdsarc.u-strasbg.fr (130.79.128.5) or via
http://cdsweb.u-strasbg.fr/cgi-bin/qcat?J/A+A/399/1083

can use the techniques developed for the IRAS-CO comparison to compare any catalogued data set with the OGS-BKP data. Section 3 compares the IRAS-CO associations found in this study to the extensive targeted study of WB89. In Sect. 4 we describe three brief studies which demonstrate the utility of the new IRAS-CO association table. Finally, conclusions are presented in Sect. 5.

2. Data

As part of the incorporation of the OGS into the Canadian Galactic Plane Survey (CGPS, Taylor et al. 2003) the original OGS was reprocessed (Brunt & Ontkean 2003, in preparation). This reprocessing removed correlated noise signals (see Heyer et al. 1998), suppressed the effects of unclean reference positions and corrected incorrectly placed spectra from the first OGS release. The OGS data were convolved to 100.″44 resolution and converted onto a standard CGPS coordinate grid prior to release as a CGPS data product. The typical sensitivity of the reprocessed OGS data is 0.17 K at 100.″44 resolution. The reprocessed OGS data cubes, along with all of the other CGPS data sets, are publicly available through the Canadian Astronomy Data Centre (CADC)[1].

As a cursory inspection of any of the OGS data cubes will reveal, the CO emission in the outer Galaxy is highly structured and quite extensive. To facilitate the comparison of the OGS data with other large databases a cloud catalogue was constructed (BKP) that describes the OGS data in terms of discrete *lbv* structures (i.e. CO "clouds"). BKP used the 100.″44 resolution data on the original OGS 50.″22 grid but after conversion onto the 0.824 km s^{-1} CGPS spectroscopic grid. The BKP catalogue was generated using a two-phase object identification algorithm. In the first phase, all contiguous *lbv* structures consisting of at least 4 voxels over which the observed radiation temperature exceeded 0.8 K were identified. The second phase of the algorithm further decomposed these (sometimes very large) structures into smaller regions of localized CO emission enhancements, using an enhanced version of the CLUMPFIND algorithm (Williams et al. 1994). This procedure leads to a high resolution discretization of the data which is critical for accurately associating CO emission with specific sources seen at other wavelengths. There are 14 592 objects contained in the BKP catalogue.

The IRAS point source catalogue (PSC) was used to obtain positional information on all of the IRAS PSC sources ("IRAS sources" hereafter) in the OGS survey region. In total there are 6698 IRAS sources in the OGS region of which 4315 have detectable CO along the line of sight as accounted for in the BKP catalogue. Even in the outer Galaxy, the widespread distribution of CO emission means that for any given IRAS source there is a chance that non-associated CO emission could be detected along the line of sight and that multiple emission components along the line of sight will occur. The latter problem was recognized in WB89 and qualitative criteria were developed to determine which of the multiple CO components along the line of sight were more likely associated with the IRAS source. However, since full maps of the CO distribution around the IRAS source position were not available there was no way to quantitatively rank the quality of a given IRAS-CO association.

BKP developed a statistical source association method that exploits the spatial information in the OGS in order to discriminate between multiple CO detections. They examined the frequency with which 10^6 randomly chosen lines of sight within the OGS region coincided with CO emission incorporated into the BKP catalogue, and occurred within an angular offset of δr arcminutes from an object with peak temperature exceeding $T_{\rm p}$ kelvins[2]. From the observed number of associations, $N_{\rm obs}(\leq\delta r,\ \geq T_{\rm p})$, they defined the expected number of associations, $N_{\rm E}(\leq\delta r,\ \geq T_{\rm p})$, that would be made towards a random position within the OGS boundaries:

$$N_{\rm E}(\leq\delta r,\ \geq T_{\rm p}) \quad = \quad N_{\rm obs}(\leq\delta r,\ \geq T_{\rm p})/N_{\rm test}$$

where $N_{\rm test} = 10^6$. [3] BKP showed that 52% of lines of sight through the OGS region will encounter CO emission in excess of 0.8 K, so it is useful to evaluate the quality of an IRAS-CO association using BKP's derived $N_{\rm E}$ values. As one would expect, large δr – low $T_{\rm p}$ "associations" are more likely (i.e. have higher $N_{\rm E}$) in the random sample than low δr – high $T_{\rm p}$ associations. For IRAS sources, we can examine the spatial offset and peak temperature of all possible CO associations and assign an $N_{\rm E}$ value accordingly. Chance associations will generally have high $N_{\rm E}$, while the close spatial coincidence (low δr) of a cloud with high $T_{\rm p}$ would have low $N_{\rm E}$, and indicate a physically interesting association.

The OGS data at each IRAS source position was examined for CO emission that is accounted for by the BKP catalogue[4]. For each IRAS-CO coincidence, the δr-$T_{\rm p}$ values were determined and an $N_{\rm E}$ value was assigned. For IRAS sources with only one possible CO association, the $N_{\rm E}$ value provides a quantitative measure of the likelihood of a true association. Multiple associations along a given line of sight were ranked by their $N_{\rm E}$ value and the cloud with the lowest $N_{\rm E}$ was taken to be the most likely true IRAS-CO association (see e.g., Fig. 1). We did not discard the other possibilities; these were retained in an $N_{\rm E}$-ordered list for each IRAS source.

Determining the absolute level of the $N_{\rm E}$ values where one would consider the IRAS-CO association to be true is more ambiguous and will often vary depending upon the sort of object one is looking at (e.g. Kerton 2002). Often additional information can be utilized to help determine the level at which the majority of the associations are non-random. Section 4.1 in this paper provides a concrete example of this for the case of an investigation of candidate zone-of-avoidance galaxies (ZOAGs).

[1] `http://cadcwww.hia.nrc.ca`

[2] The angular offset from the test position was defined as either the offset of the object's peak temperature position or the offset of the object's centroid position, whichever was closest.

[3] In the case that, at most, only one object is present along any line of sight, $N_{\rm E}(\leq\delta r,\ \geq T_{\rm p})$ would always be $\leq$1 and would be the *probability* of chance association within δr, above $T_{\rm p}$. However, this is not the case; $N_{\rm E}(\leq\delta r,\ \geq T_{\rm p})$ is thus an expectation value, and could exceed unity.

[4] We use the "ON CLOUD" method of BKP, which requires that the OGS data be examined for detected emission – see Appendix.

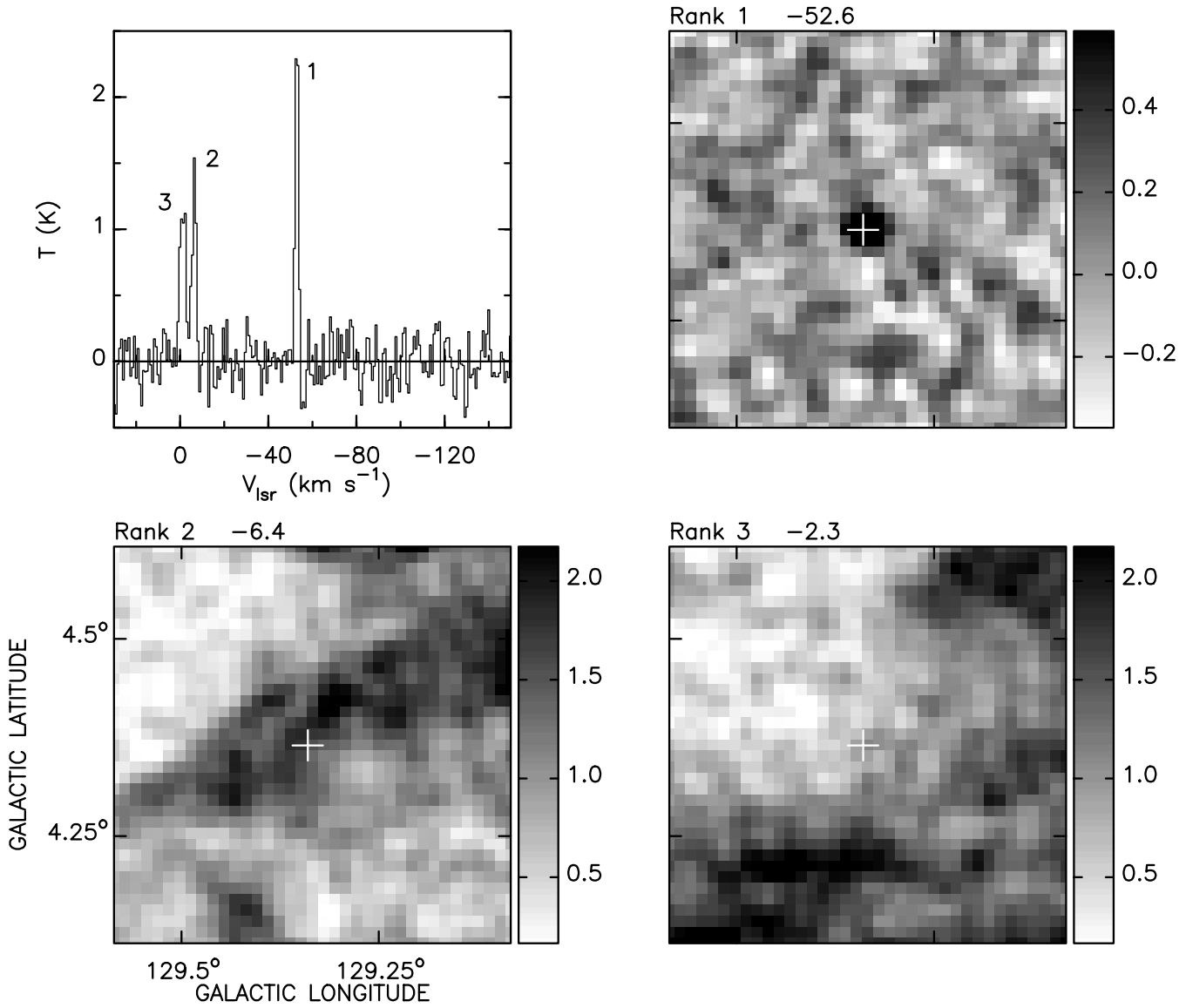

Fig. 1. Multiple CO emission components. The upper left panel shows the CO spectrum towards IRAS 01522+6611 along with the N_E ranking of each of the three components along this line of sight. The other three panels show the corresponding CO maps at the velocity indicated above each panel. The white cross indicates the position of IRAS 01522+6611. N_E values are 0.0065, 0.3454, and 0.4877 for rank 1, 2, and 3 respectively.

In addition to the difficulty in establishing a useful absolute N_E level, there are three sources of confusion in this scheme. First a "type 0" error arises when no CO detection is made towards an IRAS source due to the CO emission being either weak or very small in extent (e.g., WB89 298, see Sect. 3). A "type 1" error arises when a spuriously low N_E value is assigned to a cloud that is not physically associated with the IRAS source; this will be of particular concern if a true physical association with a different cloud is masked. As an example of a type 1 error, consider a true physical association of an IRAS source with a far outer Galaxy molecular cloud. Since emission from the distant cloud is often weak, a chance association with a nearby cloud at comparably low δr but higher T_p will result in the nearby cloud achieving a higher rank in the N_E-ordered list. A "type 2" error occurs when a true physical association of an IRAS source and a molecular cloud is assigned a spuriously high N_E value. The thresholding scheme used by BKP identified emission enhancements in the OGS data only if they were distinguishable from their surroundings by at least 0.8 K. This threshold is relatively high ($\sim 4.7\sigma$) compared with the noise level in the data to avoid inclusion of spurious clouds in the catalog. However, such a high threshold can result in lack of precision on small scales, arising from less pronounced emission enhancements being incorporated into larger, composite structures; a particular example of this is given in Sect. 3. Since we retain all possible IRAS-CO associations in our list, no true associations are discarded but they may be hidden by the influence of type 1 and 2 errors on the assigned N_E and relative rank.

Table 1 contains the main result of this paper – an N_E ordered list of all the IRAS-CO associations within the OGS. The first column of the table contains a running number of IRAS-CO associations followed by the IRAS source name (Cols. 2 and 3), position in Galactic coordinates (Cols. 4 and 5) and flux

Table 1. IRAS-CO associations.

This table is available only in electronic form at the CDS
http://cdsweb.u-strasbg.fr/cgi-bin/qcat?J/A+A/399/1083

Table 2. IRAS sources with no CO associations.

This table is available only in electronic form at the CDS
http://cdsweb.u-strasbg.fr/cgi-bin/qcat?J/A+A/399/1083

density information (flux densities in Cols. 6–9 for 12, 25, 60 and 100 μm respectively; percentage errors for the respective flux densities in Cols. 10–13). Column 14 indicates if the following offsets refer to the CO cloud peak or centroid position. Columns 15 to 21 contain information about the CO cloud. The CO peak/centroid position in Galactic coordinates and the $V_{\rm lsr}$ is given in Cols. 15–17, followed by the peak temperature ($T_{\rm p}$; Col. 18), the CO temperature at the IRAS source position (Col. 19), the angular offset between the IRAS position and the CO peak (Col. 20) and the BKP number of the cloud (Col. 21). The BKP number can be used to access the BKP catalogue where more detailed information about the CO cloud can be found. Finally Cols. 22–24 provide the $N_{\rm E}$ value (Col. 22) the relative $N_{\rm E}$ ranking (Col. 23) and the WB89 catalogue number if applicable (Col. 24). Note that the WB89 number is indicated only if CO was detected towards the IRAS source by WB89. A more detailed description of the format and contents of the machine-readable table is given in the header of the electronic version.

Also provided in this paper is a listing of the IRAS sources within the OGS that do not have associated CO as accounted for by the BKP catalogue (see Table 2). The columns in Table 2 are the same as the first 13 columns of Table 1.

The IRAS-CO association table contains a comprehensive account of the star-forming molecular ISM in the OGS region of the Galaxy that can be examined by itself or as a starting point for other investigations. In the next section we analyze the contents of the table and compare it to the results of the extensive WB89 targeted survey.

3. Analysis

It is not the intent of the paper to attempt to examine in detail every IRAS-CO source in Table 1. Rather in this section we conduct a general analysis of the objects contained in the table in terms of their IRAS colours and their $N_{\rm E}$ values to give the reader some appreciation for the overall content. In Table 3 some basic properties of the IRAS-CO sample are summarized.

An obvious question that can be raised is how do the results of this study differ from the targeted WB89 study within the OGS region? Within the OGS region (completely encompassed by the WB89 survey region) WB89 examined 292 IRAS sources of which 255 had CO detected along the line of sight. Of the 255 WB89 associations, 244 are matched by a rank = 1 BKP association (~96%). In 6 of the other cases (WB89 200, 287, 321, 376, 392, and 460) the BKP catalogue does include the WB89 associated CO but we assign it a lower ranking based upon the relative $N_{\rm E}$ values of the various CO clouds along the line of sight. For the remaining 5 cases (WB89 298, 365, 378, 398, and 439) there is no BKP cloud associated with the WB89 CO component, because it is either too faint or has too small a spatial extent (see Sect. 2 of BKP for details of the cloud selection criteria). For four of these sources (WB89 365, 378, 398, and 439) we associate, with $N_{\rm E} \geq 0.1$ in all cases, another CO cloud along the line of sight with the IRAS source. This leaves us with 4061 other IRAS-CO objects to investigate – what are these objects? A histogram showing the distribution of $N_{\rm E}$ values for these objects is shown in Fig. 2 in comparison with the histogram for the 254 WB89 sources included in the BKP catalogue. The $N_{\rm E}$ bins for all of the histograms shown in this paper are evenly distributed in log space from $10^{-3.5}$ to $10^{-0.5}$. Clearly some of our 4061 IRAS-CO sources are spurious IRAS-CO associations as suggested by the much larger high $N_{\rm E}$ tail seen in our sample. However it is also clear that there is a substantial population of previously unexamined low $N_{\rm E}$ value IRAS-CO sources where a true IRAS-CO association is highly probable.

Table 3. IRAS-CO sources.

Number	Notes
6698	IRAS sources in the OGS region
4315	IRAS sources associated with CO emission (IRAS-CO)
2547	1 CO component
1237	2 CO components
411	3 CO components
102	4 CO components
17	5 CO components
1	6 CO components
4025	CO clouds (from BKP) associated with IRAS sources
384	IRAS-CO sources with no IRAS upper limits
541	IRAS-CO sources with one IRAS upper limit

What sorts of objects would be missed by a targeted survey like WB89? The IRAS sources examined in WB89 were selected to have no upper limits at 25, 60 and 100 μm and have colours typical of star-forming regions: $\log(25/12) > 0$, $0.38 < \log(60/25) < 1.88$, and $-0.77 < \log(100/60) < 0.39 + 0.23\log(60/25)$. The two general categories of IRAS sources that avoid these criteria are those IRAS sources with no upper limits that lie outside the WB89 colour cuts, and those IRAS sources with upper limits at 25, 60 and/or 100 μm. The next two subsections investigate these two subsets in more detail.

3.1. Good IRAS colours

In total there are 384 IRAS-CO sources (including 214 WB89 sources) with no IRAS flux density upper limits in *any* of the four bands. Figure 3 shows the distribution of $N_{\rm E}$ values for the 170 IRAS-CO objects defined in this study and the 214 WB89 objects. More of the non-targeted sample is found in the high $N_{\rm E}$ bins compared with the targeted WB89 sample; 77% of the WB89 sample is found in the first four bins

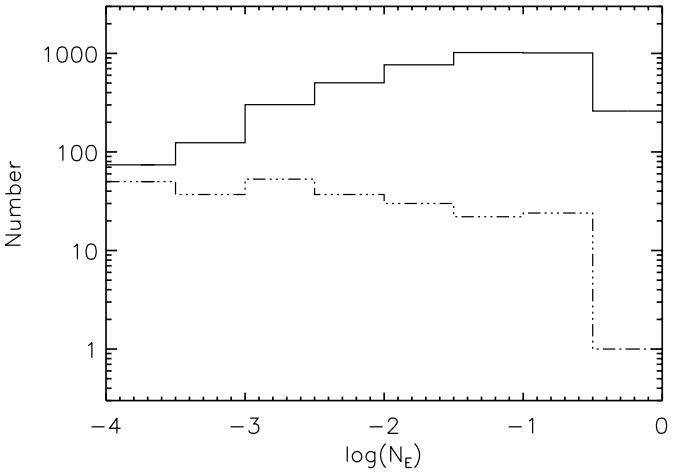

Fig. 2. Histogram showing the distribution of $N_{\rm E}$ for IRAS-CO sources. WB89 sources are shown by the dot-dash line and non-WB89 IRAS-CO sources are indicated by the solid line. Note the comparable numbers at low $N_{\rm E}$ and the large increase in non-WB89 sources at higher $N_{\rm E}$ presumably due to false IRAS-CO associations.

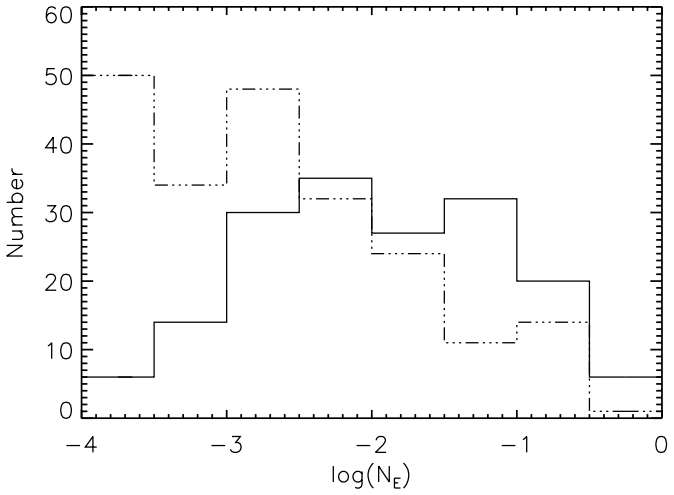

Fig. 3. Histogram for IRAS-CO sources having no IRAS flux density upper limits. The solid line shows the distribution of $N_{\rm E}$ for the 170 IRAS-CO sources defined in this study, and the dot-dash line shows the 214 WB89 sources.

compared with 50% for the non-targeted sample. The number of IRAS-CO sources in the high $N_{\rm E}$ bins ($N_{\rm E} > 0.01$) is higher for the non-targeted sample (85 objects) compared with the WB89 survey (50 objects). This is due to the targeted nature of the WB89 survey which reduces the number of probably spurious IRAS-CO associations at high $N_{\rm E}$.

Since we have four well-defined IRAS fluxes for these objects the IRAS colours can be used to make a rough identification of the types of objects. For reference, Fig. 4 shows the main regions of the IRAS 12-25-60 μm colour-colour plane occupied by various astronomical objects. As one can see in most cases the identification cannot be exact since there can be substantial overlap of objects at a given position of the plane. In Figs. 5 and 6 we show the positions in the IRAS 12-25-60 μm colour-colour plane of the non-targeted sample of 170 IRAS-CO sources for the various $N_{\rm E}$ bins, along with the applicable

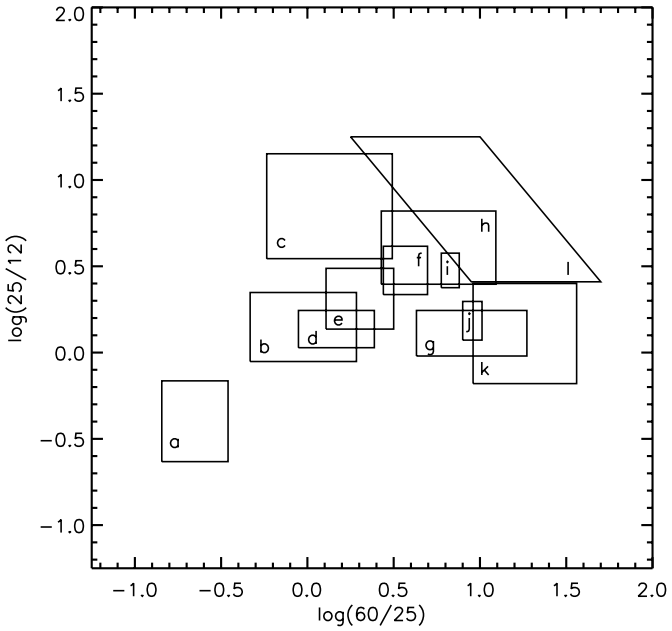

Fig. 4. Distribution of objects in the IRAS 12-25-60 μm colour plane. The boxes show the main concentrations of a variety of different astronomical objects: a – carbon stars, b – blue planetary nebulae, c – red planetary nebulae, d – T Tauri stars, e – quasars, f – Seyferts, g – blue reflection nebulae, h – red reflection nebulae, i – red galaxies, j – blue galaxies, k – embedded intermediate-mass stars, l – HII regions. a–j from Walker et al. (1989); k from Kerton (2002), l from Hughes & MacLeod (1989).

WB89 colour constraints shown as solid lines. There is a population of objects, especially in the low $N_{\rm E}$ bins, that lies in and around the WB89 colour criteria[5]. These low $N_{\rm E}$ objects are almost certainly associated with star-forming regions. As $N_{\rm E}$ increases more of the objects move away from the star-forming region area the colour-colour plane.

Since the non-targeted sample was of a manageable size we searched the SIMBAD database for any known cross-identifications along with any previous observations and/or detections of the IRAS sources with other tracers. The results of this search are summarized in Table 4. In the two lowest $N_{\rm E}$ bins the majority of the objects are either unstudied or poorly studied, however the two known objects are both Galactic – the HII region GLMP 1072 (Garcia-Lario et al. 1997) and the PP1 nebula (Parsamian & Petrosian 1979). As you move to higher $N_{\rm E}$ values one starts to see more stellar sources entering the sample – these are in most cases spurious associations, as will be discussed below, but there are also a few known Galactic HII regions in the sample confirming that some true IRAS-CO associations can be found at the $N_{\rm E} \sim 0.01$ level. It is at this level that the first known extragalactic sources start to appear. If we just take the objects in the two lowest bins ($N_{\rm E} \leq 10^{-3}$) as being likely star-forming regions (because of their low $N_{\rm E}$ and the fact their IR colours are very close to the WB89 colours) we obtain a sample of 18 new objects,

[5] If they lie within the WB89 region, they were not included in the WB89 sample because they failed the log(100/60) colour constraint not shown in the figures.

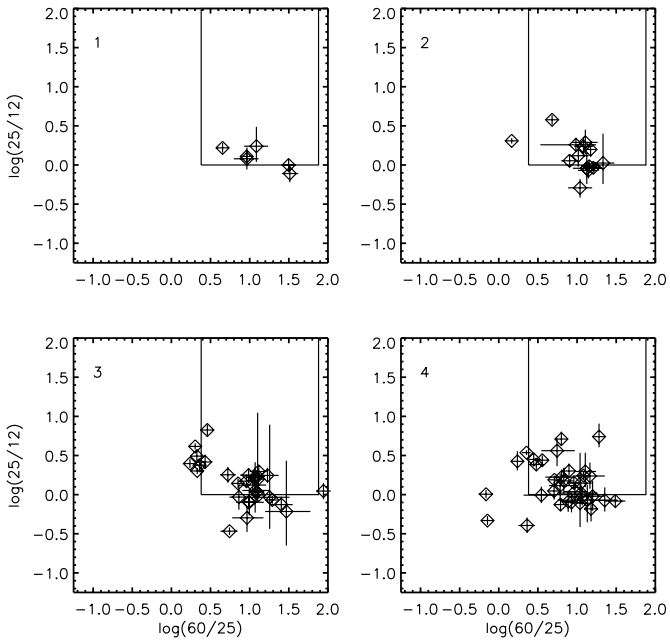

Fig. 5. IRAS 12-25-60 μm colour plane. IRAS-CO sources with no IRAS flux density upper limits and not included in the WB89 study are plotted for the four lowest $N_{\rm E}$ bins. Bins are indicated by the number in the upper left of each panel: 1- $N_{\rm E} \leq 10^{-3.5}$, 2- $10^{-3.5} < N_{\rm E} \leq 10^{-3.0}$, 3- $10^{-3.0} < N_{\rm E} \leq 10^{-2.5}$, 4- $10^{-2.5} < N_{\rm E} \leq 10^{-2.0}$. The solid lines indicate the WB89 colour criteria representative of star forming regions.

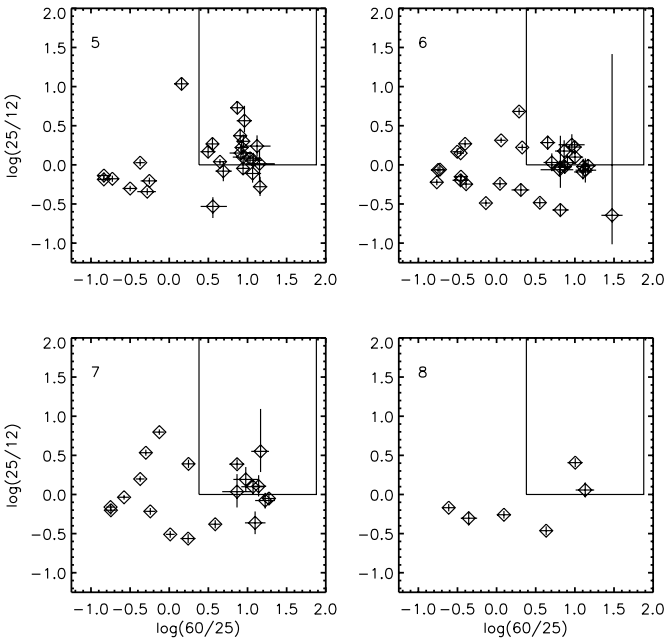

Fig. 6. IRAS 12-25-60 μm colour plane. As Fig. 5 for the four highest $N_{\rm E}$ bins. Bins are indicated by the number in the upper left of each panel: 5- $10^{-2.0} < N_{\rm E} \leq 10^{-1.5}$, 6- $10^{-1.5} < N_{\rm E} \leq 10^{-1.0}$, 7- $10^{-1.0} < N_{\rm E} \leq 10^{-0.5}$, 8- $10^{-0.5} < N_{\rm E}$.

an increase of ∼21% over the 84 WB89 sources found in the same two bins. Alternatively, since most of the non-stellar known Galactic objects are associated with star forming regions, for each bin we can use the ratio of the number of known Galactic objects:total number of known objects to select the same fraction of unknown objects as likely star forming regions. Doing this we obtain a sample of 55 objects (assuming the ratio = 1 for both of the lowest $N_{\rm E}$ bins), an increase of ∼22% over the entire WB89 sample. We note that while such an analysis does not identify the star-forming regions in question explicitly it does single out a subsample of IRAS sources where star forming regions are likely to be discovered and as such can provide a good starting point for further studies.

To gain further insight into the range of the quality of the IRAS-CO associations spanned by this sample we examined the contents of the highest and lowest $N_{\rm E}$ bins in more detail (see Table 5). For the highest bin (number 8, see Fig. 7) there is one unambiguous random IRAS-CO association – IRAS 02381+5923 (topmost point in the Bin 8 panel of Fig. 6) is emission associated with the galaxy Maffei 2. Inspection of the full catalogue entry for this object shows that the IRAS-CO association is indeed very poor – the "associated" CO is a local cloud ($V_{\rm lsr} = -2.3$) and the offset between the IRAS coordinates and the CO $T_{\rm p}$ position is 17.′3.

Three of the IRAS-CO sources in Bin 8 are stars, IRAS 02473+5738, IRAS 03008+5637 and IRAS 22197+6028 (the three leftmost points in the Bin 8 panel of Fig. 6). This fact does not immediately mean that the IRAS-CO association is spurious as CO emission has been observed towards AGB stars where it originates from an expanding circumstellar shell of material (Kwok 2000). However, the CO lines associated with AGB stars are observed to be very broad ∼30 km s^{-1} due to the expansion motions and, since they originate in a circumstellar shell, very good positional correspondence between the CO peak position and the IRAS source is expected. IRAS 02473+5738 is a M2Iab star with a measured radial velocity of −30.9 km s^{-1}. In this case the CO association is clearly random as the radial velocity of the associated CO cloud is only −12.2 km s^{-1}. In addition the CO cloud (BKP 4486) has a linewidth of only 1.54 km s^{-1}. IRAS 03008+5637 is a known M9 AGB star. It has an "E-type" IRAS-LRS spectrum where the 9.7 μm silicate dust feature is in emission thus implying the star is an oxygen-rich AGB with a relatively optically thin circumstellar envelope (Kwok et al. 1997). The cloud associated with IRAS 03008+5637, BKP 12070, has a linewidth of only 1.78 km s^{-1} and thus is also a spurious association. Finally for IRAS 22197+6028 the linewidth of the associated CO cloud is again too narrow (3.2 km s^{-1}) to be a believable CO association. We conclude that all of the stellar CO associations here are spurious.

The remaining two sources, IRAS 00040+6645 and IRAS 03118+6058, are more curious. IRAS 03118+6058 (lowest point in the Bin 8 panel of Fig. 6) was examined by Wouterloot et al. (1993) for H_2O, OH, CH_3OH emission with no detections. There is no 21 cm continuum emission visible in CGPS images of the region. DSS images of the object show that there is nothing exactly at the position of the IRAS source but the carbon star Kiso C5- 65 (Maehara & Soyano 1991) is just within the error ellipse of the position of IRAS 03118+6058 (19″ × 3″ at 68°). Based upon the highly negative log(25/12) colour and the proximity of a known

Table 4. Good IRAS colours – SIMBAD results.

N_E Bin[a]		Known Objects			Unknown Objects	
Low	High	Star[b]	Galactic[c]	Extragal.	No det.[d]	Not Studied
	$10^{-3.5}$	0	0	0	3	3
$10^{-3.5}$	$10^{-3.0}$	0	2	0	5	7
$10^{-3.0}$	$10^{-2.5}$	2	6	1	11	10
$10^{-2.5}$	$10^{-2.0}$	4	5	0	11	15
$10^{-2.0}$	$10^{-1.5}$	4	3	1	6	13
$10^{-1.5}$	$10^{-1.0}$	13	2	0	4	13
$10^{-1.0}$	$10^{-0.5}$	10	1	0	6	3
$10^{-0.5}$		3	0	1	1	1
All Bins		36	19	3	47	65

[a] Bins cover Low $< N_E \leq$ High.
[b] Star refers primarily to AGB stars.
[c] E.g., HII regions, reflection nebulae.
[d] Examined for other gas tracers but no detections made.

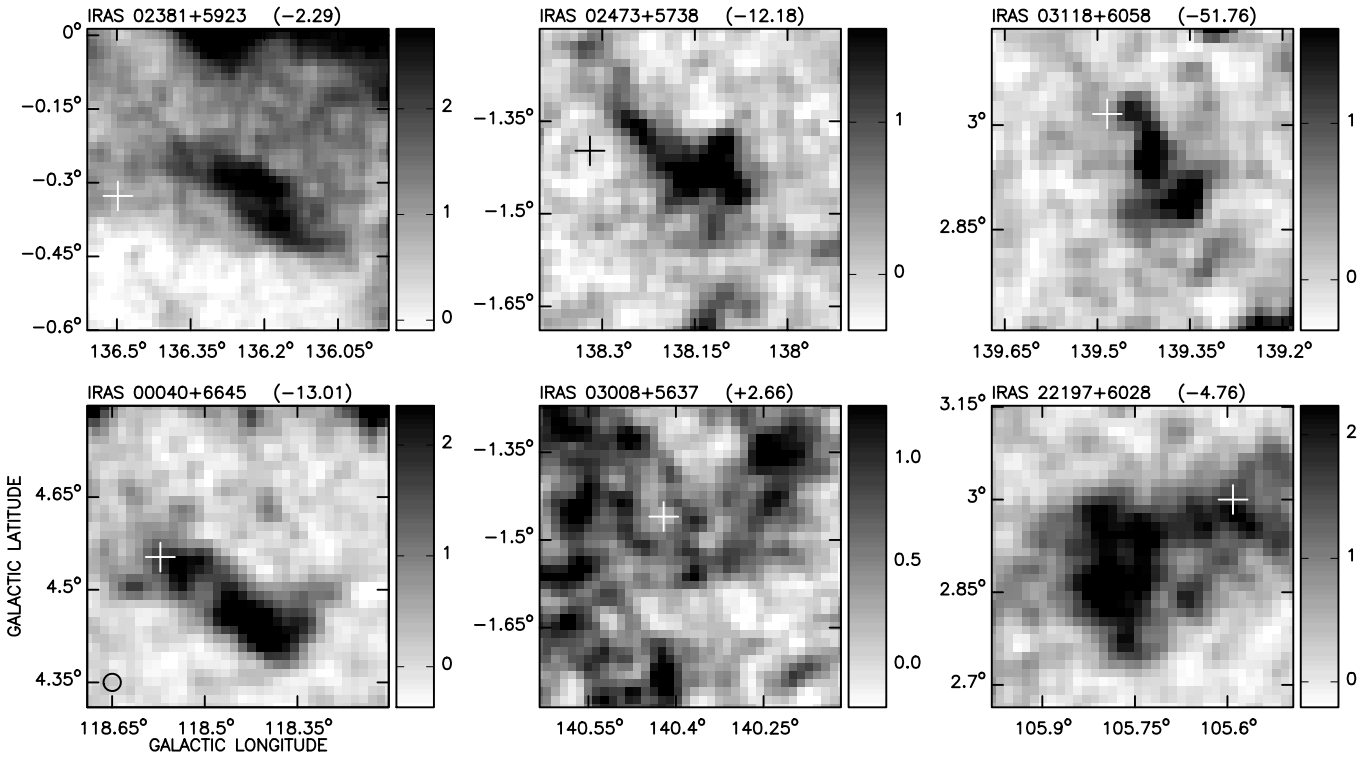

Fig. 7. Maps of CO emission for the IRAS-CO sources having no flux density upper limits and $N_E > 10^{-0.5}$ (Bin 8). The greyscale shows CO emission (K) in the peak channel (the V_{lsr} (km s^{-1}) for the channel is indicated in parentheses above each panel). The white crosses indicate the position of the IRAS source identified above each panel.

carbon star, we conclude that IRAS 03118+6058 is the carbon star Kiso C5- 65 and that the IRAS-CO association is spurious. Finally, IRAS 00040+6645 falls within the WB89 12-25-60 μm colour criteria and has associated extended Midcourse Space Experiment (MSX, Price et al. 2001) Band A (8.3 μm) emission (see Fig. 8). The associated CO cloud has $V_{lsr} \sim -13$ km s^{-1} which is consistent with it being associated with the nearby Sh 2–171 region (Yang & Fukui 1992). We conclude this object is a photodissociation region (PDR) found at the edge of a CO cloud related to Sh 2-171. This object is a good example of the "type 2" error (a false high N_E) discussed previously in Sect. 2. As is clear in Fig. 8 the associated CO cloud has peaks. The contrast between the two peaks is very low however and the algorithm did not break the cloud into separate structures. Since the IRAS source position is then compared to the more distant maximum peak of the cloud a large N_E value results. We expect this sort of error to occur primarily in some of the local, more extended, clouds. At larger distances a cloud such as this one would be a much more compact object and the δr would be significantly smaller.

In contrast, now consider the six objects found in the low N_E bin (see Fig. 9). In this case the SIMBAD search

Table 5. Good IRAS colours – $N_E \leq 10^{-3.5}$ and $N_E > 10^{-0.5}$ sources.

	IRAS	Notes
$N_E \leq 10^{-3.5}$	03062+5742	0 references
	03083+5618	WBF93 – no detection
	22451+5906	WBF93, WWH88, WW86 – no det.
	22460+6341	0 references
	23089+5914	WWH88, WW86 – no detection
	23369+6142	0 references
$N_E > 10^{-0.5}$	00040+6645	0 references , Kiso C5-65
	02381+5923	Maffei 2 galaxy
	02473+5738	HD 237010 M2Iab star
	03118+6058	WBF93 – no detection, PDR
	03008+5637	M9 AGB star
	22197+6028	V662 Cep – S star
WBF93	Wouterloot et al. (1993) – H_2O, OH, CH_3OH	
WWH88	Wouterloot et al. (1988) – NH_3	
WW86	Wouterloot & Walmsley (1986) – H_2O.	

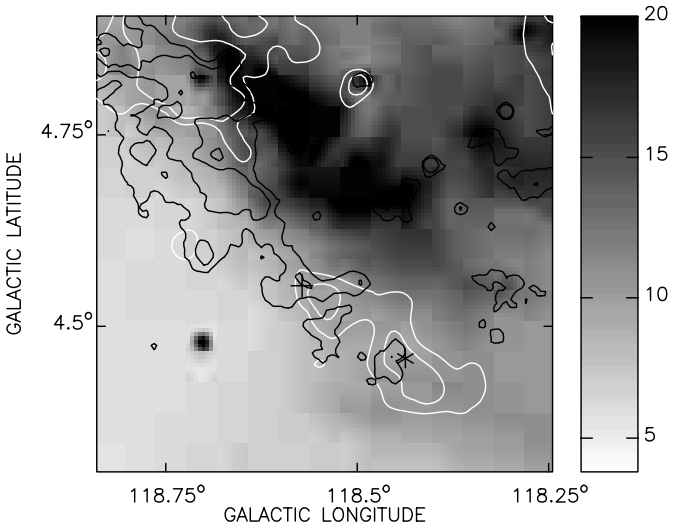

Fig. 8. IRAS 00040+6645 and Sh 2-171. Greyscale shows 21-cm radio continuum emission (K) from the eastern portion of Sh 2-171. MSX Band A (8.3 μm) emission (black contours at 1.5 and 2.5×10^{-6} W m^{-2} sr^{-1}) and integrated CO emission (white contours at 5 and 7 K km s^{-1}; integrated from −9.3 to −15.1 km s^{-1} (V_{lsr})) are overlayed. The position of IRAS 00040+6645 is indicated by the cross, and the centroid of the associated CO cloud is indicated by the asterisk. The location of the IRAS source at the edge of the CO cloud and the HII region suggests that it is a PDR.

reveals no other known cross-identifications. Three of the sources have not been investigated before and the other three have been examined for a variety of high density gas tracers but with no detections. Inspection of the IRAS colour-colour plots show that all of these objects are very close to the original WB89 colour criteria and just missed being included in their sample. Given their position in the colour-colour plane and the very good association with CO they most likely represent a sample of star-forming regions. The lack of detections in the high density gas tracers suggest they may be slightly evolved regions. Four of the objects, IRAS 22451+5906, IRAS 22460+6341, IRAS 23089+5914, and IRAS 03083+5618 have been identified as likely embedded intermediate-mass stars (Kerton 2002).

3.2. Poor IRAS colours

The remainder of the sample (3931 IRAS-CO sources) have a flux density upper limit in at least one of the IRAS bands, this includes 40 sources with upper limits in the IRAS 12 μm band included in the WB89 sample. Table 6 summarizes the N_E distribution of this sample.

It is clear from looking at the number of objects in the lower N_E bins that there is potentially a very large number of interesting objects in this sample. For this paper we will limit our analysis to the 68 sources in the $N_E \leq 10^{-3.5}$ bin. We first queried the SIMBAD database for these 68 sources. Seven of the IRAS sources were previously known objects – three HII regions, one reflection nebula, and three star-forming cores. Twenty-one of the objects had been included in other surveys for dense gas tracers but with no detections, and 40 of the IRAS sources had not been studied at all beyond their catalogue identification.

Because of the upper limits on the IRAS flux densities one cannot use the IRAS colour-colour plane to effectively look at the sources. However if we limit ourselves only to those objects with a single flux density upper limit then some progress can

Table 6. Poor IRAS colours – N_E distribution.

N_E Bin[a]				
Low	High	Non-Targeted	WB89	Total
	$10^{-3.5}$	68	0	68
$10^{-3.5}$	$10^{-3.0}$	110	3	113
$10^{-3.0}$	$10^{-2.5}$	272	5	277
$10^{-2.5}$	$10^{-2.0}$	468	5	473
$10^{-2.0}$	$10^{-1.5}$	739	6	745
$10^{-1.5}$	$10^{-1.0}$	988	11	999
$10^{-1.0}$	$10^{-0.5}$	992	10	1002
$10^{-0.5}$		254	0	254
All Bins		3891	40	3931

[a] Bins cover Low $< N_E \leq$ High.

be made. Objects with upper limits at either 12 or 100 μm can be unambiguously placed on the 25-60-100 or 12-25-60 colour plane respectively. On the other colour plane one colour can be fixed while the other will be a limit. The situation is somewhat more poor for sources with only upper limits at either 25 or 60 μm. In this case the source will have a limit in both colors and the allowed position of the point will be along a diagonal line in the colour-colour plane – not ideal but at least certain regions of the plane can be eliminated.

For the 68 very low N_E sources, 19 have a single upper limit: 3 at 12 μm, 4 at 60 μm, and 12 at 100 μm. Table 7 shows details of the objects based upon the results of a SIMBAD query and Fig. 10 shows this subsample of IRAS-CO sources in both IRAS colour planes. Examining the 12-25-60 μm plane in more detail we see that 11 of the 12 sources with good colours in this plane (i.e., with 100 μm upper limits) lie within

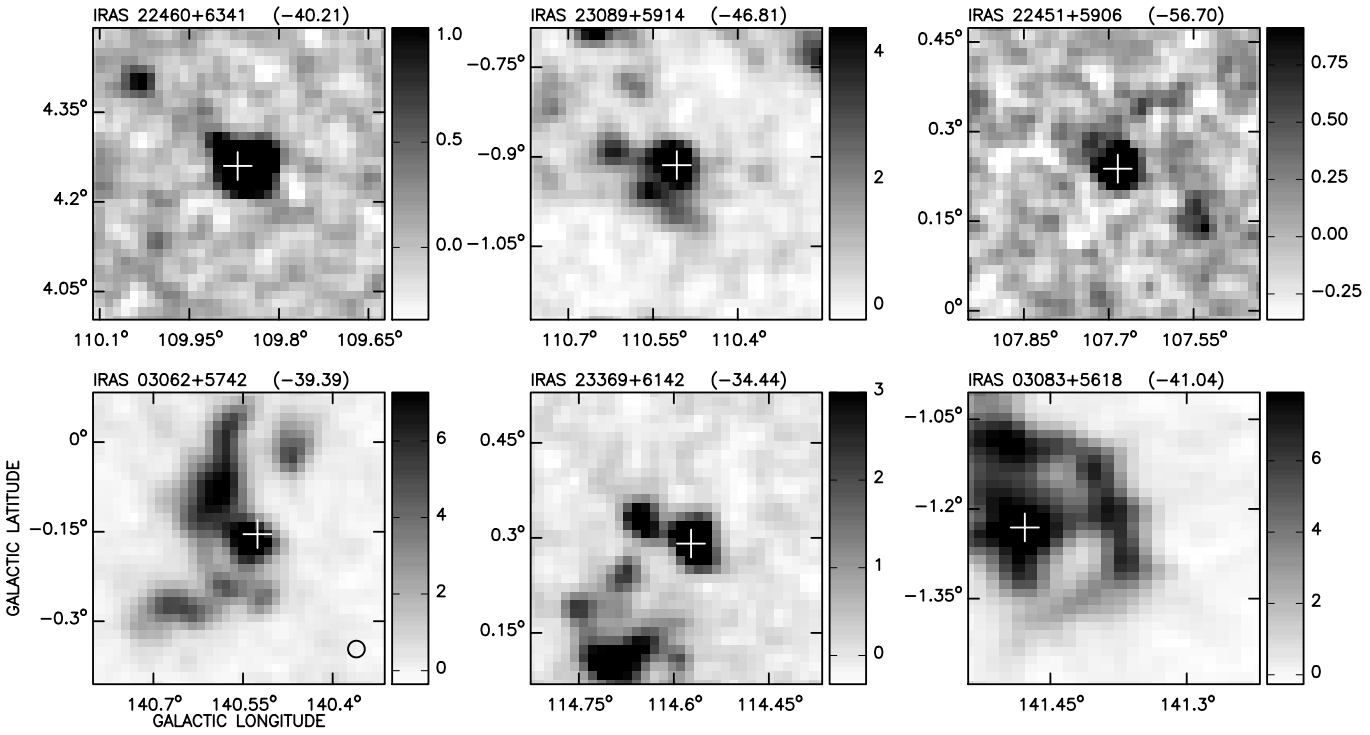

Fig. 9. IRAS-CO sources with no IRAS flux density upper limits and $N_E \leq 10^{-3.5}$. The white crosses indicate the position of each IRAS source. The greyscale shows the CO emission (K) in the peak channel, and the velocity of the channel (V_{lsr} (km s^{-1})) is shown in parentheses above each panel.

the WB89 region and the other source is just outside of the WB89 region. Eight of the objects are known to be associated with star forming regions and we think it is highly likely that all twelve of these objects are associated with star-forming regions. One of the 3 12 μm upper limit sources lies within the WB89 region and all of these sources have log (60/25) colours consistent with the WB89 criteria. Given their close association with CO it is likely these are also all associated with star-forming regions. The sources with 60 μm upper limits are slightly harder to interpret. Unfortunately there are no known cross-identifications for these objects, but all of them could be associated with star formation if the upper limits are not too far off the true flux densities.

The 25-60-100 μm colour plane confirms these observations. There is not much of a surprise with the 100 μm upper limit sources since we already knew that they had log (60/25) colours consistent with WB89. We see that all of these sources could lie within or close to the WB89 region, again depending upon the true value of the 100 μm flux density. One of the 3 12 μm upper limit sources lies inside of the WB89 region and the other two lie just outside of the region and could again easily be star forming regions. As with the other colour plane the identity of the 60 μm upper limit sources depends critically upon how far off the upper limit is from the true 60 μm flux density.

3.3. IRAS sources with no CO associations

As mentioned in Sect. 2 there are 2383 IRAS sources in the OGS that are not associated with any CO emission as accounted for in the BKP catalogue. Because of the lack of associated CO we expect that most of these sources will either be stars or extragalactic sources. This idea is supported when one examines the average flux densities of the associated and non-associated IRAS sample (see Table 8). The average flux densities for the non-associated IRAS sample are significantly lower than the IRAS-CO sample.

Of the non-associated IRAS sources, only 41 have good IRAS colours in all four IRAS bands and thus can be placed on the IRAS colour plane unambiguously. Figure 11 shows these 41 objects on the 12-25-60 μm IRAS colour plane. A search of SIMBAD reveals that 15 of the objects are stars, and 2 are known planetary nebulae. Also, even though a number of these objects occupy regions of the colour-colour plane consistent with star forming regions, the SIMBAD search reveals no known star forming regions in this sample. These objects are most likely galaxies or red reflection nebulae (see Fig. 4). For the former we do not expect to observe associated CO in the V_{lsr} range of the survey while the latter objects are fairly evolved objects where a CO association is not highly probable. In this region of the colour-colour plane the lack of associated CO is thus a very useful means to remove the degeneracy present in the IRAS colour identification. Section 4.1 provides an example of using the presence or lack of a CO association to clarify the true nature of an object.

4. Applications

In this section we present the results of three studies that made extensive use of the IRAS-CO association table (Table 1). The purpose of this section is twofold – first it will give the reader

Table 7. $N_E \leq 10^{-3.5}$, single upper limit sources.

IRAS	Limit[a]	Notes[b]
00206+6555	100	UCHII region – BNM96 CS(2-1) det.
02157+6053	100	K01 – submm sources
02227+6127	100	K02 – embedded B star
02570+6028	100	CHS00 – embedded cluster
03054+6407	100	
22111+5845	100	S00 – no det.
22163+5555	100	K02 – embedded B star
22333+5744	100	K02 – embedded B star
23033+5951	100	UCHII region – BNM96 CS(2-1) det.
23140+6042	100	WWH88, WW86 – no det
23377+6059	100	
23483+6325	100	K02 – embedded B star
22510+6153	60	WBF93, WWH88, WW86 – no det.
22521+6205	60	WBF93, WWH88, WW86 – no det.
00153+6532	60	
03116+5951	60	
00510+6550	12	
02366+5845	12	WBF93 no det.
02499+5752	12	

[a] IRAS band (μm) with flux density upper limit.

[b] Blank indicates unstudied object;
BNM96 – Bronfman et al. (1996),
K01 – Kerton et al. (2001),
K02 – Kerton (2002),
S00 – Szymczak et al. (2000),
other abbreviations as in Table 5.

Table 8. Average IRAS flux density comparison.

	Average Flux Density	
IRAS Band	IRAS-CO Sample[a]	No CO Association[b]
$< F_{12} >$	2.42 ± 0.28[c]	2.14 ± 0.04
$< F_{25} >$	5.52 ± 1.4	1.59 ± 0.03
$< F_{60} >$	40.79 ± 8.05	2.39 ± 0.05
$< F_{100} >$	114.90 ± 16.59	21.14 ± 0.4

[a] 4315 IRAS sources.

[b] 2383 IRAS sources.

[c] standard error of the mean.

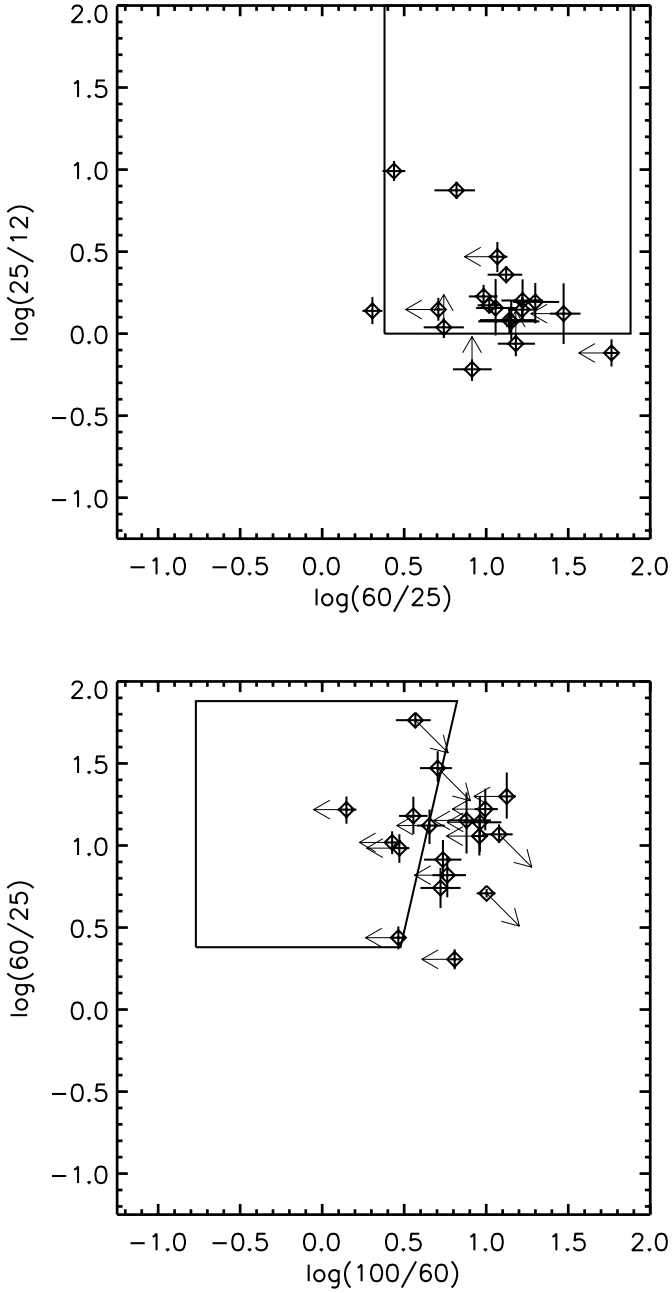

Fig. 10. IRAS colour-colour planes showing IRAS-CO sources with $N_E \leq 10^{-3.5}$ and one IRAS flux density upper limit. The solid lines show the WB89 colour criteria representative of star forming regions. Arrows indicate the effect of the single flux density upper limit on the IRAS colour.

a sense of how Table 1 can be utilized in practice, and second it presents some interesting results from our initial application of the table to some astronomical studies.

4.1. ZOAGs and Galactic Nebulae

The Galactic zone-of-avoidance (ZOA) is the low galactic latitude portion of the sky where extinction due to dust in our Galaxy makes the optical detection of galaxies very difficult. A common, and surprisingly productive, way to detect galaxies in this region is to visually inspect the Palomar Observatory Sky Survey (POSS) plates for non-stellar objects at low galactic latitude. As a result of such studies there now exists a large compilation of optically identified zone-of-avoidance galaxies (ZOAGs) in the literature (Weinberger et al. 1999; Seeberger & Saurer 1998, and references therein). It has been recognized though that the observed nebulosities cannot be easily differentiated from Galactic nebulosities (Weinberger et al. 1999)

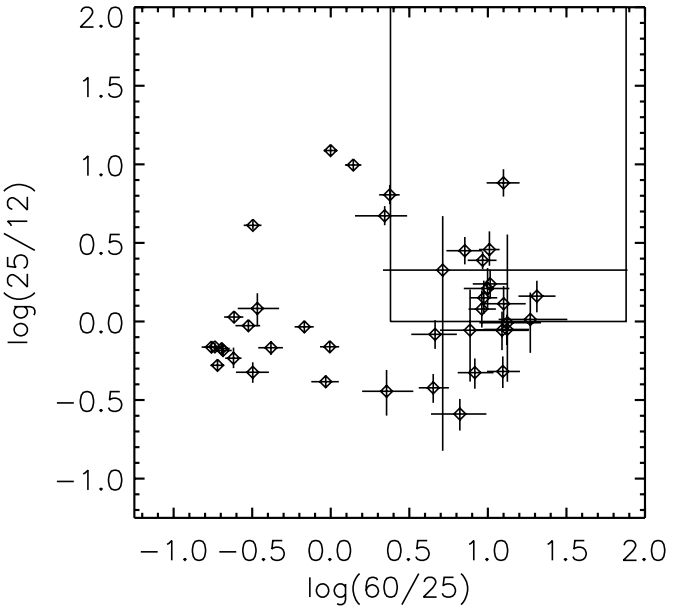

Fig. 11. IRAS sources with no flux density upper limits and no CO associations. Many of the objects plotted in this 12-25-60 μm colour plane are obviously stellar objects where one does not expect associated CO. For objects near and within the WB89 colour criteria (shown as the solid lines) the lack of CO emission indicates that the objects are most likely not star forming regions in our Galaxy.

thus the possibility that the ZOAG identification is spurious is more likely when there is an associated IRAS source (expected for a Galactic star forming region). To investigate the occurrence of false ZOAG identifications we compiled a list of all of the ZOAGs with IRAS sources contained in the OGS survey region. From this list we looked at which of the ZOAGs had associated CO. In total there are 56 ZOAGs with IRAS associations in the OGS region. Each of the objects was investigated using SIMBAD to determine if there was any more information on the object beyond the optical identification on the POSS plates. We found that 17 of the ZOAGs had another identification; four of the ZOAGs were definitively shown to be Galactic regions and 13 of the ZOAGs were definitively shown to be extra-galactic (primarily from a measured HI velocity). This extra piece of information allowed us to calibrate the $N_{\rm E}$ values for the remaining objects. All of the known Galactic objects have $N_{\rm E} \leq 0.0028$ while all of the known extra-galactic objects have $N_{\rm E} \geq 0.0253$ (see Table 9).

Of the remaining 39 objects (see Tables 10 and 11), 12 have no CO associations and thus we conclude they are good ZOAG candidates. The remaining 27 objects with CO associations were sorted by $N_{\rm E}$. Seven of these putative ZOAGs had $N_{\rm E} \leq 0.0028$ and are probably Galactic nebulae, while 17 ZOAGs had $N_{\rm E} \geq 0.0253$ and are probably correctly identified as extragalactic objects. Three of the objects fell between these two limits defined by the known object sample. While their $N_{\rm E}$ values tend to be closer to the Galactic sample we looked for further information from other datasets to help decide if the objects were Galactic or not.

First we looked at whether or not the 56 ZOAGs were MSX Band A ($\sim$8.3 μm) sources and if they had any associated 21 cm radio continuum emission using the continuum images from the CGPS. All of the known Galactic sources were strong MSX sources with no 21 cm continuum emission except for some weak emission from the distant HII region IRAS 02421+6233. In contrast all of the known extragalactic sources have associated 21cm continuum emission and all but one (the nearby Maffei 2 galaxy) have either no or very weak MSX Band A emission. This criterion (no MSX but 21 cm continuum emission) is seen in all but one of the 17 probable extragalactic sources lending weight to the conclusion that these objects are indeed extragalactic. The pattern is also seen in most of the 12 objects that had no CO association to start with and thus were automatically assumed to be extragalactic. The three intermediate $N_{\rm E}$ sources have MSX and 21 cm continuum emission properties consistent with them being Galactic objects.

In summary, of the 56 original ZOAGs 14 (25%) of them are Galactic objects (4 previously known, 10 identified as such from the $N_{\rm E}$ analysis), and 42 (75%) of them are extragalactic (13 previously known and 29 identified in this analysis).

4.2. Far outer Galaxy CO

The study of molecular clouds and star formation in the far outer Galaxy[6] is intriguing as it allows us to examine a region of the Galaxy with different properties (metallicity, pressure) than our local region. It is not within the scope of this paper to perform a detailed analysis of all of the far outer Galaxy molecular clouds within the OGS so for purposes of illustration we will restrict the analysis to those clouds with $V_{\rm lsr} < -100$ km s^{-1}. Over the range of the OGS this corresponds to Galactocentric distances ranging from >20 kpc at the high longitude end to $\sim$16 kpc at the low longitude end (e.g., see Fig. 4 of Heyer et al. 1998). We find a total of 24 BKP clouds meeting this criteria, five of which have associated IRAS sources. Included in this sample are Clouds 1 and 2 of Digel et al. (1994) and the molecular cloud associated with WB89 288, mapped in various CO lines by Brand & Wouterloot (1994). In Table 12 we list the basic properties of the clouds and Fig. 12 shows some representative images of the BKP clouds. Most of the more massive clouds in our sample have associated IRAS sources and thus have been previously investigated; however, BKP 10873 appears to be a previously unexamined large far outer Galaxy molecular cloud with $M \sim 10^4\ M_{\odot}$. There is clearly sufficient mass in this object that star-formation is certainly possible and BKP 10873 would make a worthwhile target for further higher resolution and sensitivity observations in both the millimeter and infrared.

Of particular interest are two distant CO clouds that have associated IRAS sources and have not been previously studied (see Fig. 12). IRAS 22143+6023 is associated with BKP 10889 and has a kinematically derived Galactocentric distance of $R_{\rm G} = 16.49$ kpc. The IRAS-CO association is very good with $N_{\rm E} = 0.0009$, and the cloud is the only significant

[6] Here we adopt the canonical definition of "far" as meaning objects with a Galactocentric distance of $R_{\rm G} > 16$ kpc.

Table 9. ZOAGs with IRAS counterparts in the OGS – known objects.

ZOAG	IRAS	BKP	N_E	MSX	C21	Notes
Galactic						
131.86+01.33	02071+6235	10684	0.0028	Y	N	HII Region (1)
135.63+02.77	02421+6233	10578	0.0009	Y	Y	HII Region (1)
136.39+02.27	02461+6147	7537	0.0003	Y	N	−42.4 (2)
118.97+01.89	00117+6412	6687	0.0002	Y	N	−36.2 (2)
Extragalactic with CO association						
136.50-00.33	02381+5923	12354	0.4952	Y	Y	−17, Maffei 2
132.78+03.68	02217+6430	11399	0.3833	N	Y	+12145 (3)
129.83+03.28	01542+6500	11733	0.2389	N	Y	+10493 (3)
134.22+04.05	02354+6418	11680	0.1590	N	Y	+5306 (3)
136.27-01.91	02317+5801	12271	0.1267	N	Y	+5650, Wein 20 (4)
133.83+03.40	02297+6351	11872	0.1228	N	Y	+4202 (3)
138.96+02.66	03067+6055	12924	0.0921	Y(weak)	Y	+2350 (5)
127.05-02.58	01211+5946	13339	0.0663	N	Y	+17678 (3)
107.13+03.41	22287+6137	2088	0.0253	Y (weak)	Y	+3503 (6)
Extragalactic without CO association						
129.64+02.58	01509+6423	...	...	N	Y	+10461 (3)
130.20+03.90	01591+6531	...	...	N	Y	+9593 (3)
135.64+02.43	02410+6215	...	...	Y (weak)	Y	+13191 (1) Seyfert 1
138.52-00.11	02530+5843	...	...	N	Y	Dwingeloo 1

(1) – Rudolph et al. (1996).
(2) – Bronfman et al. (1996), CS(2-1) LSR velocity shown.
(3) – Nakanishi et al. (1997), redshift (cz, in km s^{-1}) shown.
(4) – Pfleiderer et al. (1981), redshift (cz, in km s^{-1}) shown.
(5) – Hau et al. (1995), redshift (cz, in km s^{-1}) shown.
(6) – Weinberger et al. (1995), redshift (cz, in km s^{-1}) shown.

CO emission along this line of sight. The IRAS flux densities are low as one would expect for a distant source: 0.22, 0.25, 1.45 and 14.27 Jy at 12, 25, 60 and 100 μm respectively. While there are upper limits at 25 and 100 μm, the 12 and 60 μm flux densities do indicate that the spectrum is rising into the far-infrared. We thus identify IRAS 22143+6023 as a new far outer Galaxy star forming region.

IRAS 23482+6524 is another possible far outer Galaxy star forming region. In this case there are no IRAS flux density upper limits and the spectrum is rising through to 100 μm: 0.37, 0.35, 4.04, and 32.16 Jy at 12, 25, 60 and 100 μm respectively. The association with BKP 10898 has an N_E of 0.0035. There is also another possible CO association at −60 km s^{-1} but with a very high N_E = 0.1601.

In brief, our initial exploration of the BKP catalog and the IRAS-CO association table has led to the discovery of two new candidate far outer Galaxy star forming regions and a large distant molecular cloud that shows no signs of massive star formation.

4.3. Bright CO clouds with no IRAS sources

An interesting question one can ask is whether or not there are any very bright CO clouds in the survey region that do not have any associated IRAS sources and thus are not currently associated with star formation. For this example, we define a "very bright" CO cloud as one having a peak CO brightness temperature $T_p \geq 10$ K. This is a very small subset of the CO clouds we find in the outer Galaxy. Of the 14592 BKP CO clouds only 120 (0.8%) have $T_p \geq 10$ K and, of these, 114 (95%) have IRAS associations at the rank = 1 (111 clouds) or rank = 2 (three clouds) level. This is clearly a special population as only 28% of the entire BKP sample have associated IRAS sources at any rank. The properties of the six very bright clouds with no IRAS sources are tabulated in Table 13. The cloud masses range from a few hundred to a few thousand $M_\odot$.

A careful examination of the positions of these sources reveals that they are not randomly distributed in the OGS region, rather we find that these objects are found at the edges of HII regions and are thus associated with PDRs. BKP 7782 is found

Table 10. ZOAGs with IRAS counterparts in the OGS – Unknown Objects – 1.

ZOAG	IRAS	BKP	N_E	MSX	C21	Notes
No CO Association - Probable Extragalactic						
102.24-01.89	22184+5432	...	...	N	Y	Wein 7 (1)
124.21-02.87	00585+5942	...	...	N	N	...
129.90-01.32	01455+6031	...	...	N	Y	...
131.18+03.40	02068+6445	...	...	N	N	...
131.42+05.27	02146+6627	...	...	...	Y	...
131.48+02.72	02075+6401	...	...	N	Y	...
135.90-02.25	02280+5751	...	...	N	Y	...
137.17-02.92	02348+5644	...	...	N	N	...
139.52+04.53	03189+6213	...	...	N	Y	...
141.52+02.97	03256+5949	...	...	N	Y	...
141.85+04.95	03370+6115	...	...	N	Y	...
141.96-02.65	03061+5450	...	...	N	Y	...
CO Association – Probable extragalactic from N_E value						
134.02+04.67	02359+6457	11606	0.5307	N	Y	...
131.32+04.61	02115+6552	11749	0.4935	N	Y	...
140.41-00.39	03046+5733	12063	0.4813	N	Y	...
133.19+02.76	02222+6330	11422	0.4493	N	Y	...
125.95+02.72	01170+6509	11765	0.3921	N	Y	...
123.99+04.29	00590+6652	11301	0.3444	N	Y	...
129.98+04.96	01599+6636	11216	0.3042	N	Y	...
133.39+04.10	02283+6440	11345	0.2862	N	Y	...
129.93+03.60	01559+6518	11697	0.2528	N	Y	...
139.30+04.83	03188+6236	12987	0.2410	N	Y	...
125.73-02.19	01111+6018	13334	0.2012	N	N	...
138.24+04.06	03074+6230	13181	0.1748	N	Y	...
121.84-02.76	00397+5949	5954	0.1532	N	Y	...
115.43+05.10	23319+6633	11157	0.1418	N	Y	...
126.16-00.37	01159+6203	13272	0.0740	Y (weak)	Y	...
135.92-01.66	02299+5823	12277	0.0563	N	Y	...
138.62-00.86	02510+5759	7866	0.0338	N	Y	...

(1) – Pfleiderer et al. (1981).

at the edge of the large W4 continuum loop, BKP 11016 and 11018 are both found at the edge of the western part of Sh 2-171, BKP 13900 is on the edge of Sh 2-159, BKP 12547 is near Sh 2-155 and BKP 12127 is near Sh 2-140 (FG S140 18) (Falgarone & Gilmore 1991). High resolution (~20″) MSX Band A images were inspected to search for any signs of point-like infrared emission. In all six cases none was found; rather, clearly elongated structures associated with the ionized-molecular gas interface were seen. We suggest that these six clouds are CO clouds that are being externally heated by the nearby HII region and do not have an internal source of heat as would be suggested by the presence of an IRAS point source. We note that if T_p is substantially raised in this manner then the masses in Table 13 will be overestimates of the true mass. The location of these clouds, at the edge of various HII regions, makes them ideal targets to examine the earliest stages of star formation induced by the expansion of HII regions.

5. Conclusions

We have investigated the association of all of the IRAS sources contained within the OGS survey region with molecular material.

(1) Since we do not apply any constraints to the IRAS sources we have discovered a substantial number of previously unexamined IRAS sources that are likely to be star forming regions. For IRAS sources with no flux density upper limits we estimate that there are 55 IRAS sources not previously identified as possible star forming regions. This is an increase

Table 11. ZOAGs with IRAS counterparts in the OGS – Unknown Objects – 2.

ZOAG	IRAS	BKP	N_E	MSX	C21	Notes
CO Association – Probable Galactic from N_E value						
130.17+00.49	01511+6213	8175	0.0140	Y	N	...
116.77+01.56	23527+6328	9536	0.0089	Y	N	Wein 8 (1)
137.06+03.12	02546+6214	8779	0.0050	Y (weak)	Y (weak)	...
CO Association - Galactic from N_E value						
139.97+02.59	03134+6021	8437	0.0027	Y	N	...
134.27-01.90	02175+5845	8120	0.0026	Y	N	...
130.29+01.65	01546+6319	9296	0.0023	Y	Y (weak)	Wein 17 (1)
118.44+01.25	00080+6329	7063	0.0019	Y	N	Wein 9 (1)
133.88+02.53	02272+6302	6403	0.0009	Y	N	...
118.63-00.40	00117+6153	8501	0.0005	Y	N	
137.24+05.36	03054+6407	6073	0.0002	...	N	...

(1) – Pfleiderer et al. (1981).

Table 12. Far outer Galaxy CO clouds with $V_{lsr} < -100$ km s^{-1}.

BKP	N_{pix}[a]	l^b (°)	b^b (°)	V^b_{lsr} (km s^{-1})	T_p (K)	$R_\odot$[c] (kpc)	R_G[c] (kpc)	M[d] (10^3 $M_\odot$)	Notes
10872	86	114.338	0.780	−101.22	3.54	11.8	17.15	2	IRAS 23338+6207 WB89 288
10873	37	114.212	0.836	−102.05	1.83	12.0	17.32	10	
10877	5	131.162	1.394	−101.22	1.09	15.3	21.85	0.2	D94 Cloud 1
10878	27	109.288	2.078	−101.22	1.72	11.7	16.67	0.7	
10879	5	107.726	2.943	−101.05	1.01	11.8	16.51	0.1	
10880	6	105.243	3.012	−100.22	1.02	11.7	16.17	0.1	
10881	10	137.286	−1.159	−101.22	1.21	19.7	26.58[e]	0.6	assoc. with D94 Cloud 2
10882	7	114.282	0.655	−101.22	1.13	11.9	17.24	0.2	
10883	7	123.489	1.478	−102.05	1.04	13.1	19.15	0.2	
10884	4	121.690	2.050	−101.22	1.01	12.6	18.54	0.1	
10885	74	137.760	−0.963	−103.70	2.83	21.5	28.37[e]	8	D94 Cloud 2, IRAS 02450+5816 = YSO ~ B star (KT00)
10886	27	137.774	−1.061	−102.87	1.83	20.9	27.79[e]	2	D94 Cloud 2, IRAS 02447+5811 = PDR (KT00)
10887	4	122.289	1.687	−102.87	1.01	13.0	18.96	0.1	
10888	18	122.373	1.771	−102.87	1.14	13.0	18.96	0.5	
10889	16	104.991	3.305	−102.87	1.97	12.1	16.49	0.5	IRAS 22143+6023
10890	34	123.364	1.659	−103.70	1.37	13.4	19.42	1	
10891	6	122.345	1.924	−102.87	0.98	13.2	19.15	0.2	
10892	36	121.815	3.054	−104.52	1.35	13.2	19.10	1	
10893	6	122.736	2.371	−104.52	1.01	13.6	19.55	0.2	
10894	5	122.750	2.454	−104.52	1.02	13.5	19.46	0.1	
10895	13	122.778	2.524	−106.99	1.91	14.3	20.21	0.6	
10896	8	117.588	3.961	−106.17	1.16	13.1	18.63	0.2	
10897	4	118.146	3.417	−106.99	0.96	13.4	18.96	0.1	
10898	9	116.723	3.543	−107.82	1.27	13.3	18.73	0.3	IRAS 23482+6524

[a] Total number of *lbv* pixels in the cloud.

[b] Refers to CO cloud peak.

[c] Kinematic distances using $R_\odot = 8.5$ kpc and $V_\odot = 220$ km s^{-1}.

[d] Calculated using $X = 1.9 \times 10^{20}$ (Strong & Mattox 1996).

[e] Smartt et al. (1996) suggest 15 kpc < R_G < 19 kpc.

D94 – Digel et al. (1994); KT00 – Kobayashi & Tokunaga (2000).

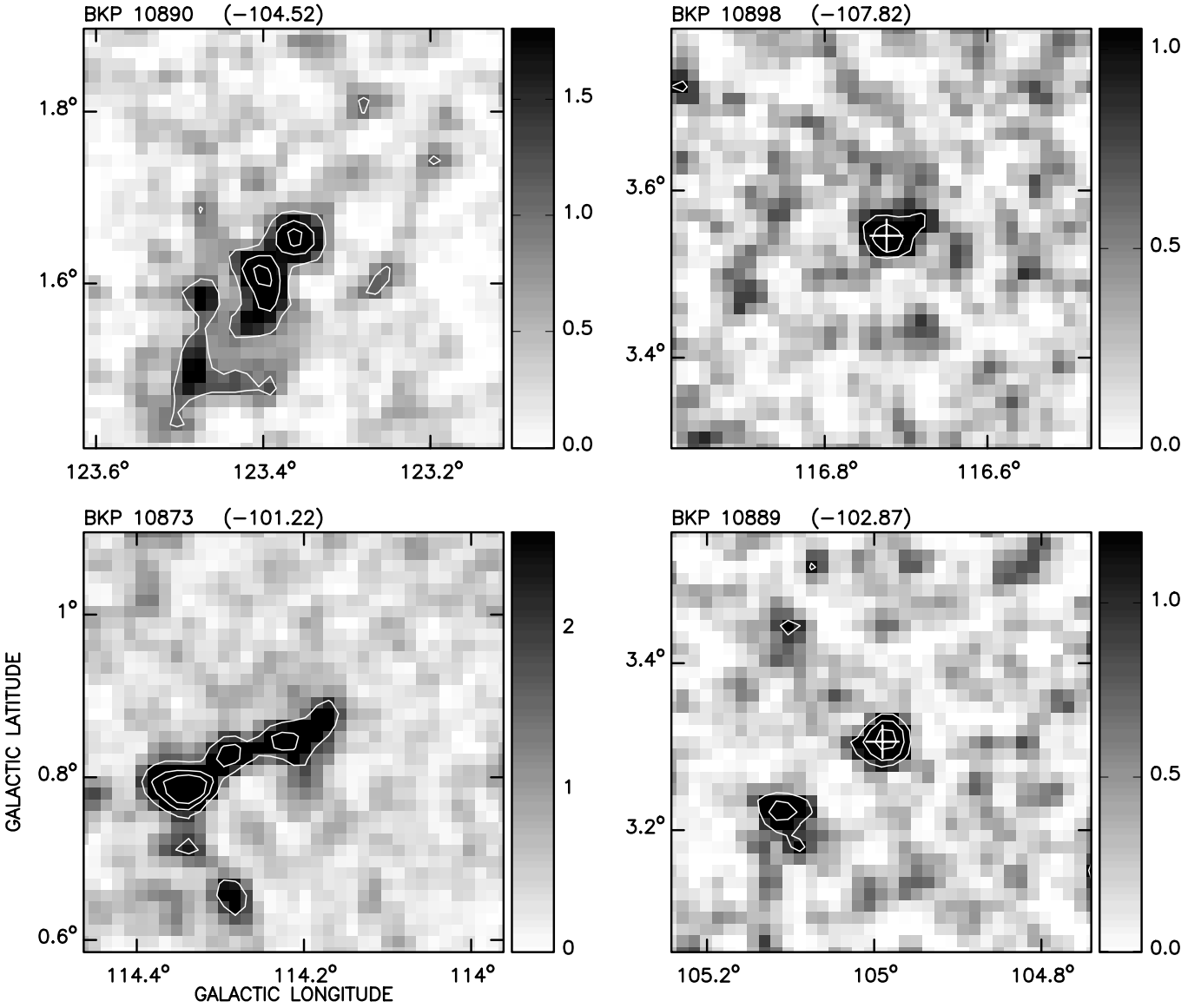

Fig. 12. Far outer Galaxy molecular clouds with and without IRAS sources. Each panel shows CO emission at the peak emission channel of the cloud (indicated in parentheses above each panel). Contours are also CO emission at the following levels: BKP 10890 – 1, 2, and 3 K; BKP 10873 – 2, 4, and 6 K; BKP 10898 – 1 and 2 K; BKP 10889 – 1, 2, and 4 K. In the two right-hand panels the crosses indicate the position of the associated IRAS source: IRAS 23482+6524 for BKP 10898, and IRAS 22143+6023 for BKP 10889.

of ~22% over previous targeted CO surveys towards IRAS sources in the OGS.

(2) By investigating the association of random lines of sight with CO emission in the OGS we were able to provide a quantitative means to judge the likelihood that any given IRAS-CO association is valid and to disentangle multiple emission components along the line of sight. The $N_{\rm E}$ table presented in this paper can be used as the basis of, or the starting point for, a number of investigations as demonstrated in Sect. 4.

(3) Our investigation of ZOAGs with associated IRAS sources has shown that about 25% of ZOAGs with IRAS associations are probably Galactic nebulae.

(4) Two new candidate far outer Galaxy star forming regions have been identified from an examination of those IRAS-CO sources associated with CO emission at $V_{\rm lsr} < -100$ km s^{-1}.

(5) Six bright CO clouds with no associated IRAS sources have been identified. All of these clouds appear to be associated with PDRs and are thus ideal targets for the investigation of the earliest stages of triggered star formation associated with HII regions.

(6) The techniques developed here to construct the IRAS-CO association table can be applied to any catalogued dataset. In the appendix we provide instructions and the necessary data to do this. We believe these techniques will only increase in applicability in the future with the continuing expansion of molecular line surveys and the increase in the number of large on-line catalogues of Galactic surveys.

Table 13. Bright CO clouds with no IRAS sources.

BKP[a]	l (°)	b (°)	$V_{\rm lsr}$ (km s^{-1})	$T_{\rm p}$ (K)	Maj. (′)	Min. (′)	$FWHM$ (km s^{-1})	$R_\odot$[b] (kpc)	M[c] (10^3 $M_\odot$)
7782	135.221	−0.015	−44.33	10.46	5.10	2.88	1.91	2.0	0.5
11016	117.937	4.854	−14.65	13.97	5.66	3.65	3.98	1.3	0.4
11018	118.104	4.686	−16.30	11.08	3.59	3.36	2.16	1.5	0.2
12127	107.140	4.965	−7.24	11.18	11.12	4.84	2.27	0.9	0.3
12547	109.860	2.203	−9.71	11.11	6.02	5.12	2.33	1.0	0.3
13900	111.785	0.362	−54.23	12.58	8.12	3.88	3.41	3.0	5.0

[a] All cloud properties except $R_\odot$ and M are from the BKP catalogue.
[b] Based upon association with HII region.
[c] Calculated using $X = 1.9 \times 10^{20}$ (Strong & Mattox 1996).

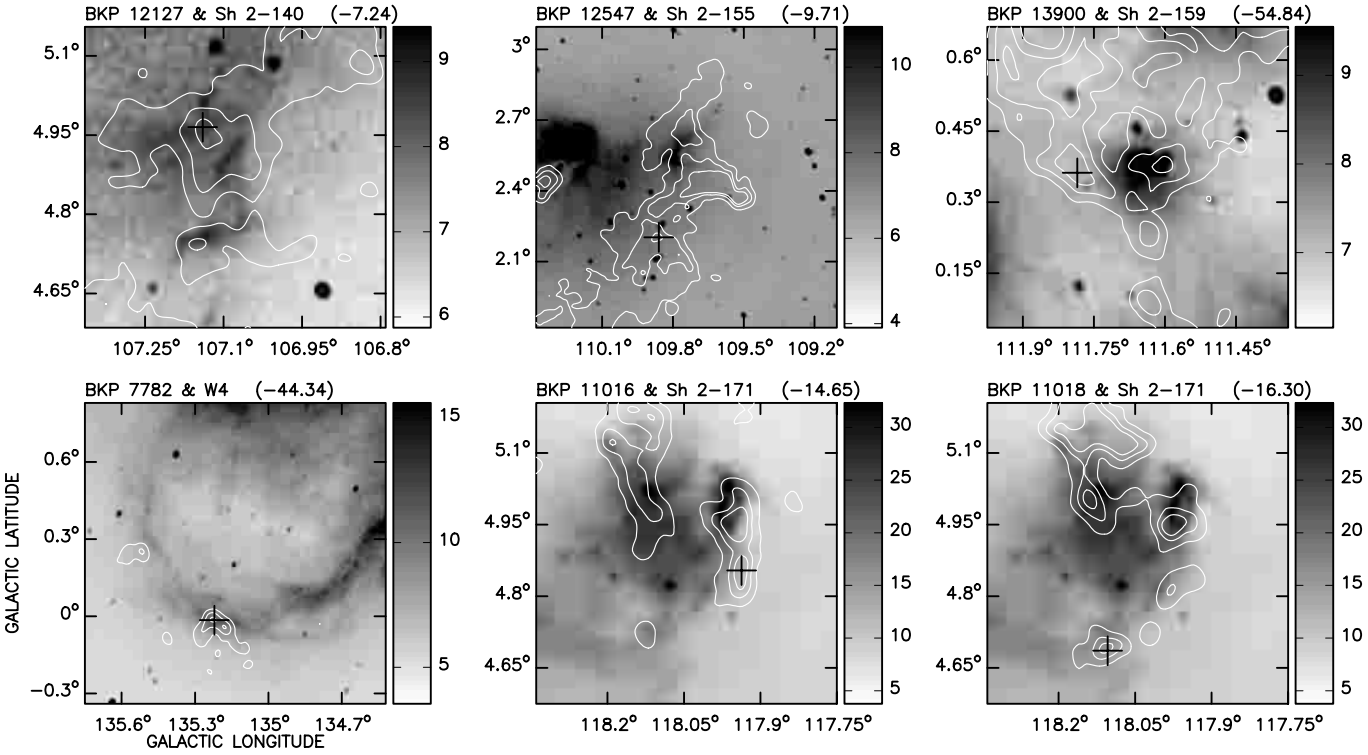

Fig. 13. Bright CO clouds with no associated IRAS sources. Greyscale shows 21 cm radio continuum emission (K) from the CGPS; contours show CO emission in the peak channel (at 2, 6, and 10 K, peak channel velocity is shown in parentheses above each panel), and crosses indicate the CO cloud peak position. All of the clouds are found close to known HII regions as indicated above each panel.

Acknowledgements. The Canadian Galactic Plane Survey is a Canadian project with international partners, and is supported by the Natural Sciences and Engineering Research Council (NSERC).

This research has made use of the SIMBAD database, operated at CDS, Strasbourg, France.

C.B. is supported by a grant from NSERC.

Appendix A: Application of $N_{\rm E}$ values to other catalogues

Obviously the IRAS catalogue is only one data set that can be compared with the distribution of molecular material in the outer Galaxy as seen in the OGS. To facilitate the comparison of other data sets with the OGS data we provide here a machine-readable table containing $N_{\rm E}$ values for δr-$T_{\rm p}$ pairs at 0.′5 and 0.5 K spacing respectively. This table is a subset of the data used to create the $N_{\rm E}$ contour plots in BKP (see their Fig. 17). We have used two different ways to associate a given object with a CO cloud. First, there is the technique we used in this paper to determine IRAS-CO associations (the "on cloud" method). This tests the chosen position to see if there is emission associated with CO clouds along the line of sight. As this requires access to the OGS data and the data cube defining the extent of each cloud we have developed an alternative association method that makes use only of data tabulated in the BKP catalogue – the "in box" method. In this case the chosen position is examined to see if it falls within a box that defines the *lb* boundaries of the CO clouds. As was demonstrated in

Table A.1. OGS N_E values.

This table is available only in electronic form at the CDS
http://cdsweb.u-strasbg.fr/cgi-bin/qcat?J/A+A/399/1083

Sect. 5 of BKP although the specific values of N_E are different the results of analyses using either technique are similar.

Column 1 of Table A.1 is the peak CO temperature of the cloud T_p given in steps of 0.5 K; Col. 2 contains the offset δr between the objects position and the CO cloud position given in steps of 0.′5, Col. 3 contains the N_E value if you are using the "in box" technique, and Col. 4 contains the N_E value for the "on cloud" technique. To use the table, determine first if a given object is associated with any CO (using either the "in box" or "on cloud" technique). If there is an association use the BKP catalogue to obtain a δr-T_p pair and use the table to obtain an N_E value for the association. To obtain N_E values at δr-T_p values not listed we recommend that the user linearly interpolates in log space. Variation in N_E is very smooth so this should be sufficiently accurate.

References

Brand, J., & Wouterloot, J. G. A. 1994, A&AS, 103, 503
Bronfman, L., Nyman, L.-A., & May, J. 1996, A&AS, 115, 81
Brunt, C., Kerton, C., & Pomerleau, C. 2003, ApJS, in press (BKP)
Digel, S., de Geus, E., & Thaddeus, P. 1994, ApJ, 422, 92
Falgarone, E., & Gilmore, W. 1991, A&A, 95, 32
Garcia-Lario, P., Manchado, A., Pych, W., & Pottasch, S. R. 1997, A&AS, 126, 479
Hau, G. K. T., Ferguson, H. C., Lahav, O., & Lynden-Bell, D. 1995, MNRAS, 277, 125
Heyer, M. H., Brundt, C., Snell, R. L., et al. 1998, ApJS, 115, 241
Hughes, V. A., & MacLeod, G. C. 1989, AJ, 97, 786
Kerton, C. R., Martin, P. G., Johnstone, D., & Ballantyne, D. R. 2001, ApJ, 552, 601
Kerton, C. R. 2002, AJ, 124, 3449
Kobayashi, N., & Tokunaga, A. T. 2000, ApJ, 532, 423
Kwok, S. 2000, The Origin and Evolution of Planetary Nebulae (Cambridge: Cambridge University Press)
Kwok, S., Volk, K., & Bidelman, W. P. 1997, ApJS, 112, 557
Maehara, H., & Soyano, T. 1991, Publ. Natl. Astron. Obs. Japan, 2, 203
Nakanishi, K., Takata, T., Yamada, T., et al. 1997, ApJS, 112, 245
Parsamian, E. S., & Petrosian, V. M. 1979, Soobshch. Byurakan Obs., 51, 3
Pfleiderer, J., Gruber, M. D., Velden, L., & Gruber, G. M. 1981, A&A, 102, 21
Price, S. D., Egan, M. P., Carey, S. J., Mizuno, D. R., & Kuchar, T. A. 2001, AJ, 121, 2819
Rudolph, A. L., Brand, J., de Geus, E. J., & Wouterloot, J. G. A. 1996, ApJ, 458, 653
Seeberger, R., & Saurer, W. 1998, A&AS, 127, 101
Smartt, S. J., Dufton, P. L., & Rolleston, W. R. J. 1996, A&A, 305, 164
Strong, A. W., & Mattox, J. R. 1996, A&A, 308, 21
Szymczak, M., Hrynek, G., & Kus, A. J. 2000, A&AS, 143, 269
Taylor, A. R., et al. 2003, AJ, submitted
Walker, H. J., Cohen, M., Volk, K., Wainscoat, R. J., & Schwartz, D. E. 1989, AJ, 98, 2163
Weinberger, R., Gajdosik, M., & Zanin, C. 1999, A&AS, 137, 293
Weinberger, R., Saurer, W., & Seeberger, R. 1995, A&AS, 110, 269
Williams, J. P., de Geus, E., & Blitz, L. 1994, ApJ, 428, 693
Wouterloot, J. G. A., & Brand, J. 1989, A&AS, 80, 149 (WB89)
Wouterloot, J. G. A., Brand, J., & Fiegle, K. 1993, A&AS, 98, 589
Wouterloot, J. G. A., & Walmsley, C. M. 1986, A&A, 168, 237
Wouterloot, J. G. A., Walmsely, C. M., & Henkel, C. 1988, A&A, 203, 367
Yang, J., & Fukui, Y. 1992, ApJ, 386, 618
Yang, J., Jiang, Z., Wang, M., Ju, B., & Wang, H. 2002, ApJS, 141, 157